Wavelength-Dependent, Orthogonal Photoregulation of DNA Liberation for Logic Operations

Ling Sum Liu, Hoi Man Leung, Clement Morville, Hoi Ching Chu, Jing Yi Tee, Alexandre Specht, Frédéric Bolze, Pik Kwan Lo

Wavelength-Dependent, Orthogonal Photoregulation of DNA Hybridization for DNA Logic Computation

Ling Sum Liu,‡[a] Hoi Man Leung,‡[a] Clément Morville,[b] Hoi Ching Chu,[a] Jing Yi Tee,[a] Alexandre Specht,[b] Frédéric Bolze[b*] and Pik Kwan Lo[a*]*

[a]Department of Chemistry, City University of Hong Kong, Tat Chee Avenue, Kowloon Tong, Hong Kong SAR (China), [b] Conception et Applications des Molécules Bioactives, UMR 7199 CNRS-Université de Strasbourg, Faculté de Pharmacie, 74 route du Rhin, 67401 Illkirch (France).

KEYWORDS

Photocleavage • dual light • orthogonal • DNA • logic gate

ABSTRACT

In this study, we synthesized two phosphoramidites based on (2,7-bis-{4-nitro-8-[3-(2-propyl)-styryl]}-9,9-bis-[1-(3,6-dioxaheptyl)]-fluorene (BNSF) and (4,4'-bis-{8-[4-nitro-3-(2-propyl)-styryl]}-3,3'-di-methoxybiphenyl (BNSMB) structures as visible light-cleavable linkers for oligonucleotide conjugation. In addition to commercial ultraviolet (UV) photocleavable (PC) linker, the BNSMB linker was further applied as a building component to construct photoregulated DNA devices as duplex structures which are functionalized with fluorophores and quenchers. Selective cleavage of PC and BNSMB is achieved in response to ultraviolet (UV) and visible light

irradiations as two inputs respectively. This leads to controllable dissociation of pieces of DNA fragments which is followed by changes of fluorescence emission as signal outputs in of system. By tuning the number and position of the photocleavable molecules, fluorophores and quenchers, various DNA devices were developed in which they mimic functions of Boolean logic gates and achieve logic operations in AND, OR, NOR and NAND gates in response to two different wavelengths of light inputs. By sequence design, the photolysis products can be precisely programmed in DNA devices and triggered release in a selective or sequential manner. Thus, this photoregulated DNA device shows potentials as a wavelength dependent drug delivery system for selective control over the release of multiple individual therapeutic oligonucleotide-based drugs. We believe that our work not only enriches the library of photocleavable phosphoramidite available for bio-conjugation, but also pave the way of developing spatiotemporal-controlled, orthogonal regulated DNA-based logic circuits for a range of applications in materials science, polymer, chemistry and biology.

1. Introduction

Silicon-based computational systems have been utilized in every aspect of human life due to their excellent information storage and computing power.[1,2] So far, the top-down approach has been used to fabricate silicon chips, but they will be very soon reaching their physical limits according to Moore's Law.[3,4] Alternatively, the bottom-up approach has been explored to construct molecular devices that can be operated using external stimuli (input) and generate some signals (outputs) for the continuous increase in computational power in various application scenarios. In the past decades, logic devices based on organic and inorganic molecules or molecular assemblies were widely introduced and studied.[5,6] Among different materials, DNA (deoxyribonucleic acid) molecules have recently drawn much attention as outstanding components in the construction of molecular logic gates because of their unique predictability of base pairing, ease of chemical synthesis, parallel processing capabilities, excellent data storage capacity, and flexibility in design.[7,8] In particular, the unique information processing and storage capabilities of

DNA not only are critical to life sciences but also signposts a promising direction for a new generation of manmade information and control nanotechnologies. Several studies have recently demonstrated that DNA-based logic gates can successfully replace the conventional silica-based logic gates for information computing, encryption, and concealment.[9–11] Thus, it is believed that DNA logic gates can potentially address the bottleneck problem of conventional logic circuits based on semiconductors in terms of operation speed of silicon materials, which is difficult to further improve. Adleman first reported the use of DNA to construct a logic gate system to solve a complicated mathematical problem in 1994.[12] Since then, researchers have started to design and create a large variety of nucleic acid-based logic gates as general computational devices, which mimic the precise control and organization of electronic systems for DNA computing, molecular sensing, disease diagnostics, and biomarker etection.[5] So far, these DNA-based logic systems could simply be controlled using stimuli including metal ions,[13,14] small molecules,[15] pH,16,17 aptamers,18,19 and sequence-defined oligonucleotides.[20–22] Delicate designs on DNA enable the formation of various functional motifs, which can provide responses to different stimuli for molecular operations.[7,8] For example, Li et al. developed a wedge-like DNA logic circuit, which was composed of OR and AND gates based on the working principle of toehold-mediated strand displacement reactions.[23] Chen and co-workers built a set of label-free and enzyme-free logic gates using the G-quadruplex as a signal transducer to generate a visible output signal. Formation of the G-quadruplex could catalyze the oxidation of 3,3′,5,5′-tetramethylbenzidine (TMB) by H2O2 in the presence of hemin to further induce a color change from colorless to blue.[24] Molecular beacons (MBs) are also widely employed functional DNA structures for the construction of DNA logic gates. Their output signals are generated after the conformational changes of the designed oligonucleotides to MB structures. Based on this principle, Park's team designed a universal single-stranded MB probe labeled with a dye and quencher for a complete set of logic gates and multilevel circuits. The suppression and restoration of fluorescence resulting from the input of different oligonucleotide sequences acted as the output signals.[25] However, a great limitation in the current DNA-based logic gate design is the lack of direct interactions with lights for real-time response. By comparison, light is the most promising noninvasive regulating input because it remotely controls the reaction systems with high spatial and temporal precision with no

pollution.[26] The traditional silicon-based computing devices typically rely on electrical signals transported via mechanical wires on the semiconductors, generating a large amount of heat. In contrast, optical signals can be rapidly delivered as pulses, even on the femtosecond time scale, by remote control, while output signals can be acquired instantaneously. In this regard, very little to no heat will be generated in the optical DNA-based systems. This will result in enhancing the reliability of the systems by avoiding the variables arising from other exogenous stimuli. Furthermore, parameters such as excitation wavelength, light power, and exposure time can be simply adjusted to regulate the photoresponsive activity. In recent years, researchers have devoted considerable effort toward developing diverse light-activated DNA logic gate systems as synthetic chemical circuits based on several strategies including nucleic acid hybridization,*27* toehold- mediated strand displacement,[28,29] aptamer ligand binding,[30] and catalytic DNAs.[31] Deiters's group constructed a variety of logic gates with AND, NOT, NAND, and NOR functions with light as the input.[32,33] Their method involved the light-induced cleavage of 6-nitropipernyloxymethylene caging groups, which were installed on thymidine nucleotides in DNA strands, to restore DNA oligonucleotide's activities for the toehold strand displacement reaction. Alternatively, Xing et al. employed the insertion of a UV-cleavable nitrobenzyl linker within the oligonucleotide backbone to regulate the conformational change of the DNA-based AND logic device to further control the dynamic assembly of high-ordered DNA nanostructures.[27] Upon UV irradiation, the photolabile molecule is cleaved, followed by dissociation of short oligonucleotides for activating or inactivating its functions. For example, Li et al. also demonstrated the photorelease of small molecules, proteins, and nanoparticles from a DNA origami-based molecular platform operated with a DNAzyme-mediated logic gate.[31] Recently, Pei's group designed intermolecular CG-C+ triple- based DNA structures in the presence of spiropyran as light-activated DNA-switching circuits for controlling computation functions.[34] After exposure to UV irradiation followed by proton transfer from CG-C+, the C–O binding of spiropyran was cleaved, and then, it was isomerized into ring-opened merocyanine. This would result in structural transition of the DNA switch from triple to duplex conformations to inhibit the strand displacement process. More recently, researchers have put much effort on the light-activated DNA nanodevices to move forward for applications in cellular environments.[30,35] These photochemical stimuli could generally narrow the gap between silicon-based circuits and

DNA-based logic devices using light to precisely control logic functions. However, the reported photochemical control of oligonucleotide activities is highly restricted to the use of single wavelength of light irradiation at 365 nm for UV-induced structural transformation or bond cleavage of caging molecules. Over the past years, development of wavelength-selective, photocontrollable logic gate systems was still in its infancy. As the systems are sensitive to multiple wavelengths of excitation light, multiwavelength-excited systems could be developed based on DNA nanotechnology for potential applications in display devices, optical information storage, and camouflage technology.[36] Furthermore, light-activated logic systems may find potential applications in the areas of remote interrogation and sensing such as lock-in detection. A very high signal-to- noise discrimination would be achievable if a single output is observed after the application of light inputs at different wavelengths. Prokup et al. developed a light-triggered AND gate through uncaging of caged thymidine nucleotides followed by a toehold-mediated strand displacement cascade in a DNA-based logic gate in response to two light irradiations at 365 and 532 nm.[28] However, the input of 532 nm overlaps with the excitation wavelength of the reporter tetramethylrhodamine; this strategy is limited when designing other logic gates. Recently, our group also reported a photon-activated, triangular-shaped 2D DNA device to emulate the operation of an OR gate. Two photon-cleavable molecules, namely 1-(2- nitrophenyl)-ethyl (2-NP) derivative and 4-nitro-4′-phenoxy-1,1′-biphenyl (4-NB) derivative, were simultaneously introduced into the system. Under light irradiation at 365 or 740 nm, the photocleavage of (2-NP) and/or 4-NB compounds results in the phototriggered release of two different pieces of fluorophore-labeled DNA strands from quenchers, restoring their detectable fluorescence signals.37 However, orthogonal activation of these two photolabile molecules for controlled release is not possible due to the chromophore of 4-NB having overlapping absorbance bands with those of 2-NP. These reported studies lack diversities and highly limit their applications for the development of photoactivated DNA computation systems with a full set of logic gate functions. To enhance the orthogonality in logic operations, functionalization of DNA oligonucleotides with photoresponsive molecules sensitive to specific wavelengths of light is highly necessary to regulate their hybridization activity in the circuit systems. Here, we first design and synthesize two new phosphoramidites based on 2,7-bis-{4-nitro-8-[3-(2-propyl)-styryl]}-9,9-bis-[1-(3,6-dioxaheptyl)]-fluorene (BNSF) and 4,4′-bis-{8-[4-nitro-3-(2-propyl)-styryl]}-3,3′-di-

methoxybiphenyl (BNSMB) motifs for DNA conjugation via standard cyanoethylphosphoramidite chemistry and further investigate their qualitative and quantitative analyses on photolysis efficiency. Subsequently, wavelength-dependent, photoregulated DNA devices were designed and constructed by hybridizing two DNA oligonucleotides, namely P-DNA and P-DNA′, which are functionalized with fluorophores, a quencher, and two photocleavable molecules including PC and BNSMB in different positions. After UV and/or visible light irradiations, selective cleavage of the PC spacer and BNSMB is achieved, respectively. This results in controllable dissociation of pieces of DNA fragments, followed by changes of fluorescence emission signals in the reaction systems. These DNA devices mimic the functions of Boolean logic gates and achieve logic operations in AND, OR,NOR, and NAND gates in response to two different wavelengths of light inputs.

2. Experimental Section

2.1. Materials and Reagents

All reagents were reagent grade quality and be utilized as received from Alfa Aesar, Apollo Scientific, Fluorochem, J&K Scientific, Sigma-Aldrich or TCI Chemicals. Anhydrous toluene, anhydrous acetonitrile (ACN), anhydrous dichloromethane (DCM), anhydrous diethyl ether (Et_2O), anhydrous tetrahydrofuran (THF), anhydrous pyridine, anhydrous triethylamine (Et_3N) and anhydrous dimethylformamide (DMF) were purchased and utilized as received from Alfa Aesar, J&K Scientific, Sigma-Aldrich or TCI Chemicals. Deuterated solvents were used as received from J&K Scientific or Sigma-Aldrich. All other solvents were technical grade unless specified. Column chromatography was performed using 60 Å 40-63-micron silica media (purchased from DAVISIL) as the solid support. The progress of column chromatography was monitored by Merck Millipore TLC silica gel 60 F254 plates, and the elutes were visualized under 254 nm and/or 365 nm UV lamp. 40% acrylamide/bis-acrylamide solution (19:1) was purchased from Bio-Rad. 1000Å nucleoside-derivatized controlled pore glass (CPG) solid support and reagents used for automated

oligonucleotide synthesis were purchased from BioAutomation. Black hole quencher-1 (BHQ) phosphormaidite, Cyanine 3 (Cy3) phosphoramidite, Cyanine 5 (Cy5) phosphoramidite, PC spacer phosphoramidite and Fluorescein (FAM) CPG were purchased from Glen Research. Sephadex G-25 (super fine DNA grade) was used as purchased from Amersham Biosciences. 1 X TBE buffer was composed of 90 mM Tris and boric acid, 1.1 mM EDTA, with a pH of 8.0 ± 0.1. 2 X TAMg buffer was composed of 80 mM tris(hydroxymethyl)aminomethane, 25 mM magnesium chloride hexahydrate and 40 mM acetic acid (glacial). The pH was adjusted to 8.0 ± 0.1 using hydrochloric acid.

2.2. Instrumentation

All NMR spectra were recorded on Bruker Ascend AVANCE III HD (BBO probe) 600 MHz NMR spectrometer, Bruker AVANCE III (BBO probe) 400 MHz NMR spectrometer or Bruker AVANCE III HD (BBO Probe) 300 MHz NMR spectrometer. ^{1}H NMR and ^{13}C NMR chemical shifts were reported in δ units, parts per million (ppm) relative to the chemical shift of residual solvents. ^{31}P NMR chemical shifts were reported in δ units, parts per million, relative to the 85% phosphoric acid as the internal standard. Electrospray ionization (ESI) mass spectrometry was performed on a PE-SCIEX API 3200 triple quadrupole mass spectrometer. Standard automated oligonucleotide solid-phase synthesis was performed on BioAutomation MerMade MM6 DNA synthesizer. Gel electrophoresis experiments were carried out on an acrylamide 20 x 20 cm Maxi Vertical electrophoresis apparatus (MV-20DSYS). Matrix-assisted laser desorption/ionization time of flight (MALDI-TOF) mass spectrometry was performed on ABI 4800 Plus MALDI TOF/TOF mass spectrometers. DHAP in 70% methanol was used as matrix. UV-Vis measurements were carried out on NanoDrop™ One (Thermofisher). One-photon photolytic uncaging was done on 415 nm or 430 nm light sources, which was achieved by using an UV

TaoYuan (415 nm, 200 mW/cm^2) or LUMOS 43 LED (430 nm, 200 mW/cm^2) LED lamps. Two-photon photolysis experiments were performed on our home-made set-up at the "Plateforme d'Imagerie Quatitative" PIQ at the faculty of pharmacy (University of Strasbourg) as described recently.[36] The excitation source was a Ti:sapphire femtosecond laser Insight DS (680-1300 nm) with pulse width < 120 fs and a repetition rate of 80 MHz (Spectra-Physics). The reference was dissolved in MeOH/H_2O 9:1 in vol. and the studied compound in PBS buffer with the absorbance of both solutions close to 0.4000 (at λ_{max}). The kinetic of the two-photon process of the compound of interest compared to the reference was studied using 80 μL of solutions (both reference and sample alternatively) irradiated and analyzed by UV-vis spectroscopy after different times of irradiation, without modifying the laser excitation settings with uncaging percentages lower than 15% to avoid interferences due to photolysis byproducts. The quadratic dependency of the photolysis percentage vs the average laser power was verified 800 nm (Figure S83) to confirm a two-photon process. HPLC analysis were performed on a high-performance chromatography system from Waters® (Waters 1525 pump with Waters 2998 photodiode array detector) equipped with a XBridge Peptide BEH C18 5-micron (4.6, 150 mm) analytical column. Spectroline® E-Series UV lamp ENF-280C/FE with 8 W output power was used in UV photolysis of logic gates. Visible light photolysis was carried out by Newport xenon light source (model of 66483-300XF-R22) with 200 W output power inserted with a 420 nm longpass filter, the transmitted wavelengths were in the range of 420-800 nm.

2.3. Synthesis of Photocleavable DNA Oligonucleotides and Reference DNA Oligonucleotides

Oligonucleotide synthesis was performed on 200 nmole scale using an automated oligonucleotide synthesizer and standard cyanoethylphosphoramidite chemistry, starting from the 1000 Å universal CPG solid support. Commercially available DNA nucleoside phosphoramidites,

BNSF phosphoramidite and BNSMB phosphoramidite were site-specifically coupled onto the growing oligonucleotides chain as an artificial base with a prolonged detritylation and coupling time. The coupling efficiency was monitored by the trityl concentration level. The DNA oligonucleotides without Cy5 fluorophore were fully deprotected in 30% ammonium hydroxide at 55°C for 16 h. The DNA oligonucleotides with Cy5 fluorophore were fully deprotected in 30% ammonium hydroxide at r.t. for 24 h.

2.4. Purification of Photocleavable DNA Oligonucleotides and Reference DNA Oligonucleotides

DNA oligonucleotides were purified on 15% polyacrylamide/8M urea polyacrylamide gels at constant current of 30 mA for 3 h (30 min at 250V followed by 2.5 h at 500 V), using 1 X TBE buffer. For DNA containing fluorophores, target bands were cut and collected in a 15 mL centrifuge tube. For DNA without fluorophores, the plates were wrapped in plastic after electrophoresis and placed on a fluorescent TLC plate and then illuminated with a UV lam at 254 nm. The bands were excised quickly. The selected gel pieces were crushed and incubated in 12 mL of sterile water at 55 °C for 16 h. The samples were concentrated to about 1 mL by speed vacuum concentrator, desalted using Sephadex G-25 column chromatography. Quantification was carried by UV-Vis analysis.

2.5. HPLC Analysis on One-photon Photolysis of Photocleavable DNA Oligonucleotides

Cy5-d15-BNSF/BNSMB-d19-FAM after irradiation of LED was subjected to reversed phase HPLC system with Waters 2998 photodiode array detector. Analysis was done by using a gradient elution starting from 100% 25 mM triethylammonium acetate (TEAA) buffer to 100% of

acetonitrile/water (v/v = 1:1) in 30 min. The signal of FAM was monitored at 495 nm and signal that of Cy5 was monitored at 650 nm. Subsequently, the quantification of photolytic products was calculated from the peaks area correlated to the calibration curves of d15 and d19-FAM.

2.6. Formation and Operation of DNA logic gates

In OR gate, **P-DNA-OR** strand was hybridized with **P-DNA-OR'** strand in a mole ratio of 1.2:1, the number of moles of **P-DNA-OR'** used was 0.11 nmol. The preparation of NOR gate was the same as OR gate. In AND gate, **P-DNA-AND** strand was hybridized with **P-DNA-AND'** strand in a mole ratio of 1.2:1, the number of moles of **P-DNA-AND'** used was 0.16 nmol. The preparation of NAND gate was same as AND gate. The mixture was prepared in 20 μL with buffer concentration of 2X TAMg and stored at 4 ^{o}C overnight. For fluorescence measurement, the samples were then diluted with 2X TAMg buffer to 120 μL prior to light irradiations. In photolysis by UV light, the samples were irradiated by an 8 W handheld UV lamp for 2 h. In photolysis by visible light, the samples were irradiated by 200 W xenon arc lamp with the 420 nm longpass filter for 1 h. Fluorescence measurement was conducted after storage at 4 ^{o}C overnight. The excitation wavelength of Cy3 was 514 nm and the emission range was collected at 550-650 nm. For gel electrophoresis, samples were prepared in 20 μL but no dilution was performed on the samples. After UV/visible light photolysis, the samples were mixed with 6.67 μL of 70% glycerol and the whole mixture was loaded to 6.5% native polyacrylamide gel in running buffer of 2X TAMg. The fluorescence of Cy3 was detected upon excitation of 532 nm and the gel was stained by Stains-All solution for visualization of bands.

2.7. Statistical Analysis

All the results were performed in triplicate and repeated for two times. Data were presented as mean ± standard deviation where applicable. Statistical analysis was conducted by one-way ANOVA with Tukey post hoc test using SPSS Statistics software.

3. Results and Discussion

3.1.Design and Synthesis of Photocleavable Phosphoramidites

The PC spacer phosphoramidite is a commercially available UV-cleavable linker for DNA conjugation. It provides high uncaging efficiency under irradiation of UV light at 365 nm. Numerous studies have demonstrated that the PC linker is feasible to synthesize photoactive DNA oligonucleotides for construction of UV-responsive DNA-based nanomaterials, which are potentially suitable for controlled drug release.[37, 39-41] However, UV light is a high-energy light source, which would result in harmful effects for long-term applications. Currently, availability of photoresponsive molecules outside the UV region is the major obstacle for building diverse DNA logic gates with dual light inputs. Coumarin derivatives are one of the most popular caged compounds with visible light activation in a physiological environment.[42-44] Introduction of substituents with electron-donating/withdrawing groups can shift the absorption wavelength of coumarin derivatives to a lower energy region.[45] Nevertheless, intermediates of recently developed coumarins are very light-sensitive and hard to be handled in the common laboratory environment.[38, 46-47] Most of the processes must be carried out in the dark. To address these problems, we are motivated to generate stable visible light-photocleavable phosphoramidites in a cost-effective way. BNSF and BNSMB derivatives were reported as efficient photoreleasing tools of glutamate and polymers.[48, 49] As reported, the synthesis of BNSF or BNSMB starts from 2,7-dibromofluorene or 4,4′-diiodo-3,3′-dimethoxybiphenyl compounds, respectively. These starting materials were reacted with 3-ethyl-4-nitrostyrene in 1:2 ratio, then followed by deprotonation and nucleophilic addition on formaldehyde to generate symmetrical and highly conjugated products. We attempted to apply the same synthetic strategy to further couple the 4,4′-dimethoxytrityl group

and phosphitylation units on these dihydroxyl-functionalized bis(stilbene) molecules BNSF and BNSMB. Unfortunately, the synthetic yields of these resulting phosphoramidites were extremely low (~5%). Indeed, the chemical syntheses reported by Nicoud and co-workers[48] cannot be effectively adapted to the preparation of phosphoramidites for oligonucleotide conjugation. Thus, we first designed and synthesized two new phosphoramidites based on BNSF and BNSMB motifs for further DNA conjugation. The detailed synthetic procedures and schemes are shown in the Supporting Information (Schemes S1–S3). The photocleavable phosphoramidites were synthesized starting from generating common molecular fragments, brominated NPPOC **3**, tritylated NPPOC **4**, and 2-cyanoethyl *N*,*N*,*N*′,*N*′-tetra*iso*propylphosphorodiamidite **5**. Then, the fluorenyl core of BNSF **8** was constructed by bromination and alkylation on the fluorene ring, and the biphenyl core of BNSMB **16** was built by successive Miyaura, Suzuki, and Sandmeyer reactions. After conversion of aromatic bromine to terminal alkene by the Heck reaction or Stille reaction, sequential intermolecular Heck reactions were performed on the fluorenyl and biphenyl cores to generate the conjugated chromophores. Finally, the synthesis of BNSF and BNSMB phosphoramidites **12** and **20** were completed by phosphitylation. The intermediates and final products were characterized by electrospray ionization mass (ESI-MS) spectrometry and ^{1}H, ^{13}C, and/or ^{31}P nuclear magnetic resonance (NMR) spectroscopies (Figures S1–S51). The data obtained were in good agreement with the proposed structures. In this work, the facile synthesis of BNSF

and BNSMB linkers is highly achieved, as their intermediates are not light-sensitive. The overall synthetic experiments can be carried out under normal environments in the laboratory.

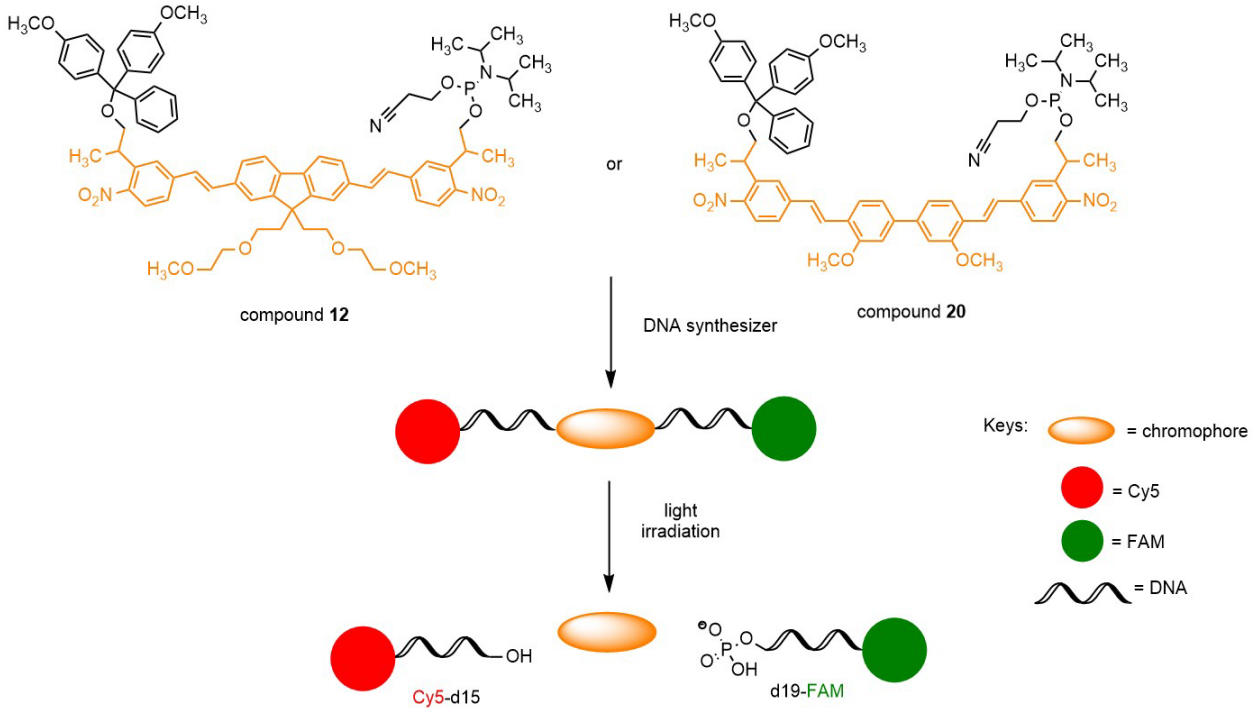

Scheme. 1 Conjugation of photocleavable phosphoramidites on DNA oligonucleotides by solid phase synthesis.

3.2.Synthesis and Characterization of Photocleavable DNA Oligonucleotides

To facilitate the characterization of fragments after photolysis, two different lengths of DNA oligonucleotides including d15 (sequence: 5′-CTGAGACTTTAATAA-3′) and d19 (sequence: 5′-TTGAAATTCACCTGGTAGC-3′) were chosen, which have already been used in our previous studies.[50,51] Commercially available cyanine 5 (Cy5) and 6-carboxyfluorescein (FAM) non-nucleosidic phosphoramidites were conjugated on the 5′ and 3′, respectively (Scheme 1). These fluorophores were utilized for the visualization of DNA fragments and increasing polarity difference between d15 and d19. The synthetic protocol of photocleavable and reference

DNA oligonucleotides was referred from our previous study.[52] The successful synthesis of DNA oligonucleotides was confirmed by matrix-assisted laser desorption/ionization time-of-flight (MALDI-TOF) mass spectrometry (Figures S52–S61). The mobilities and purities of DNA oligonucleotides were also investigated by denaturing polyacrylamide gel electrophoresis (PAGE) analysis, as shown in Figures 1a and S62. UV–Vis absorption spectroscopy studies were also performed on the BNSF- and BNSMB-conjugated DNA oligonucleotides. The maximum UV–Vis absorptions for BNSF and BNSMB were 415 and 400 nm, respectively.[48,49] As shown in Figure 1b,c, the UV–Vis absorption spectra illustrated two absorption bands at 260 nm for DNA nucleobases and at 415/400 nm for the biphenyl and fluorenyl chromophores, confirming the successful conjugation of BNSF or BNSMB motifs onto the DNA strands. The stability of DNA oligonucleotides containing BNSF and BNSMB linkers was also tested under pure water, 50 mM sodium acetate buffer at pH 4, 50 mM sodium carbonate–sodium bicarbonate buffer at pH 10, and 500 mM potassium chloride solution and at 37 °C. As characterized by denaturing gel electrophoresis, no degradation of DNA oligonucleotide was observed in each treatment (Figure S63). It is confirmed that the photocleavable linker is stable under acidic, alkaline, and high-salt content conditions and even at high temperature.

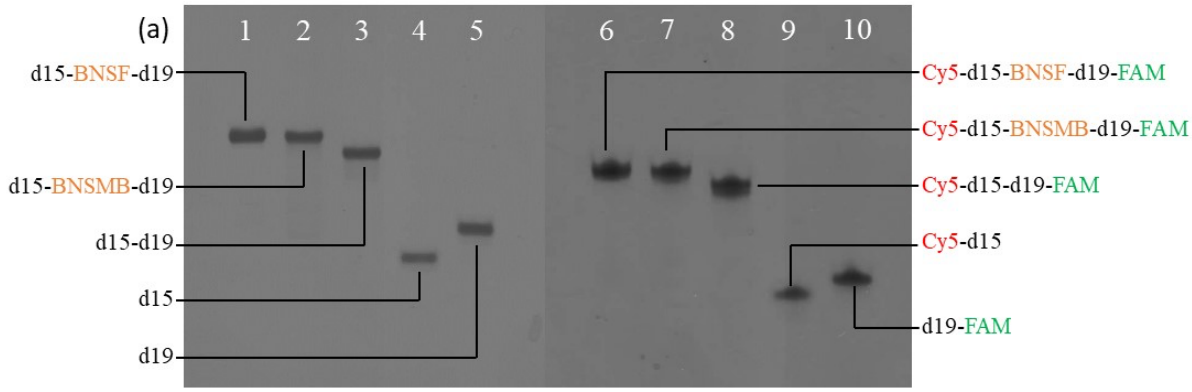

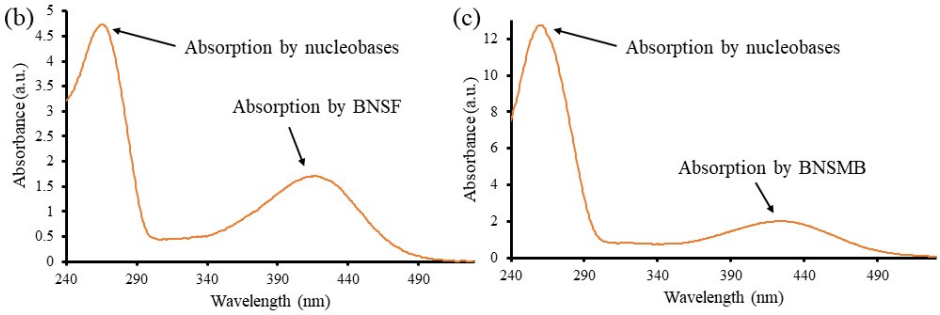

Figure 1. Characterization of the BNSF- and BNSMB- conjugated DNA oligonucleotides. (a) Denaturing PAGE analysis for mobilities and purities. (b) UV-Vis absorption spectra of (b) BNSF-conjugated and (c) BNSMB-conjugated DNA oligonucleotide.

3.3. Qualitative Analysis on the Photolysis Efficiency

Previously, effective one-photon uncaging performances of BNSF and BNSMB in glutamate and the polymer were reported.[48,49] However, the photolytic efficiency of two molecules was never reported in DNA oligonucleotides, so their photolysis was investigated qualitatively. In the literature, one-photon uncaging processes could be examined by monitoring the decreasing absorption of PPGs and increasing absorption of photolyzed products by UV–Vis spectroscopy.[38, 49, 53, 54] In our studies, one-photon induced photolysis was examined by irradiation of d15-BNSF-d19 and d15-BNSMB-d19 oligonucleotides (15 μM) at 430 nm (using a LUMOS 43 LED source from Atlas Photonics Inc.) in 1× PBS (pH 7.2). During these photolysis experiments, both caged DNA oligonucleotides showed new broad absorbance features from 300 to 600 nm, while the initial absorbance features at 405 or 415 nm gradually diminished, as shown in Figure 2a,b. Noteworthily, for longer irradiation time, the broad absorbance between 300 and 600 nm started to decrease presumably due to the instability of the BNSF and BNSMB subproducts. The samples after irradiation were also subjected to MALDI-TOF mass spectrometry analysis. As shown in Table S2 and Figures S64–S65, two peaks representing the d15 and d19 molecular fragments were

observed after irradiation of d15-BNSF-d19 and d15-BNSMB-d19 with LEDs. These UV–Vis absorption and mass spectral results were good evidence to prove the successful fragmentations on BNSF- or BNSMB-conjugated DNA oligonucleotides under irradiation with a LED light source. Further confirming the photorelease of two shorter DNAs, one-photon uncaging was done on 100 μM Cy5-d15-BNSF-d19-FAM and Cy5-d15-BNSMB-d19-FAM oligonucleotides in 2× TAMg (pH 8.0) under irradiation as a function of time. The denaturing PAGE analysis in Figure 3 revealed that the photo-uncaging of Cy5-d15-BNSF-d19-FAM and Cy5-d15-BNSMB-d19-FAM oligonucleotides could be done within 30 s using a LED to completely release the two DNA fragments. To further confirm the photolytic products, the samples after irradiation were also subjected to reversed-phase high-performance liquid chromatography (HPLC) analysis, then followed by MALDI-TOF mass spectrometry analysis. As shown in Table S3 and Figures S66–S69, mass peaks at 6395.9536 and 6399.7979 Da were found from the elutes collected at 10 min from HPLC analysis after photolysis of Cy5-d15-BNSF-d19-FAM and Cy5-d15-BNSMB-d19-FAM, respectively, confirming the release of d19-FAM. Additionally, mass peaks at 5189.9312 and 5192.2905 Da were found from the elutes collected at 17 min from HPLC analysis after photolysis of Cy5-d15-BNSF-d19-FAM and Cy5-d15-BNSMB-d19-FAM, respectively, confirming the release of Cy5-d15. In addition, it was demonstrated that d15-BNSF-d19 showed two-photon uncaging activity at 800 nm (Figure S70). Compared to PC and coumarin derivative linkers, the photocleavage of our BNSF- and BNSMB-functionalized DNA oligonucleotides results in controlled release of pure DNA fragments without other functional groups for potential biomedical applications.[55]

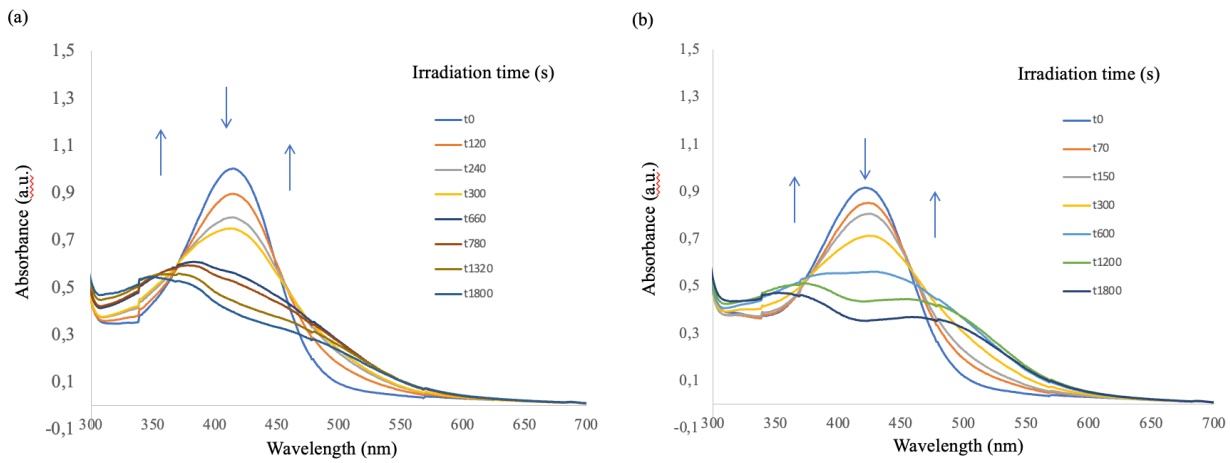

Figure 2. Variation of UV-Vis absorbance after irradiation at 430 nm of 1 mL of 15 µM solutions of samples in 1X PBS. (a) BNSF- conjugated DNA oligonucleotide (b) BNSMB- conjugated DNA oligonucleotide.

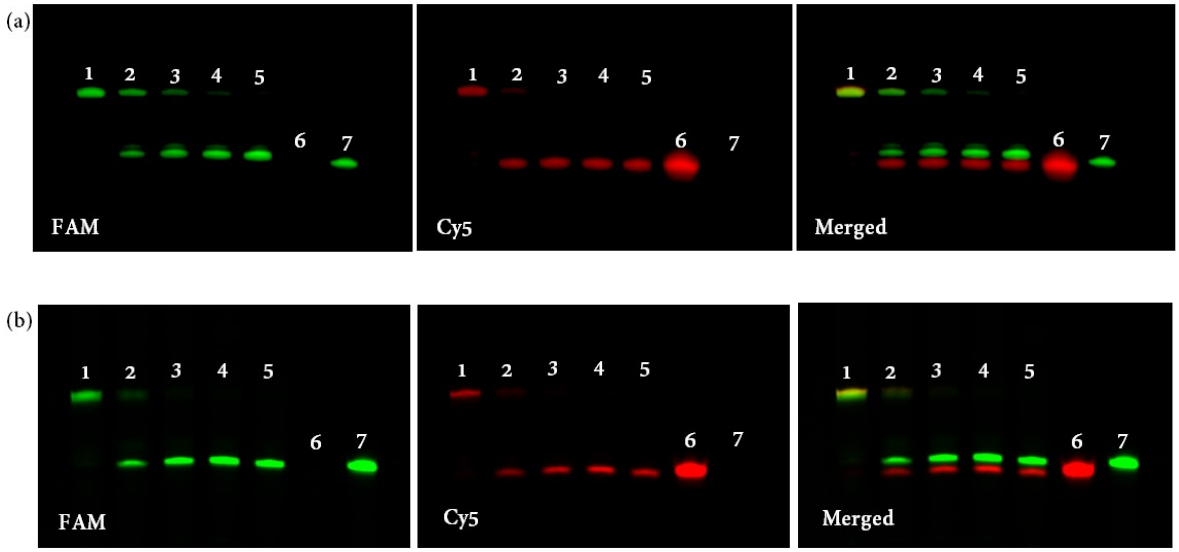

Figure 3. Denaturing PAGE analysis of (a) Cy5-d15-BNSF-d19-FAM and (b) Cy5-d15-BNSMB-d19-FAM after irradiating with 415 nm light as a function of irradiation time at 0 s (lane 1), 2 s (lane2), 5 s (lane 3), 10 s (lane 4), 30 s (lane 5). Uncaged products were compared with the Cy5-d15 (lane 6) and d19-FAM (lane 7).

3.4.Quantitative Analysis on the Photolysis Efficiency

To quantify the amount of DNA fragments released by one-photon uncaging photolysis, reversed-phase high-performance liquid chromatography (HPLC) analysis was used. By comparing the peak areas of the uncaged product and the reference standards, the quantities of uncaged products could be determined. Nevertheless, we were not able to separate the d15 and d19 oligonucleotides using reversed-phase HPLC analysis, as the retention times of d15 and d19 DNA oligonucleotides were almost identical. This may be attributed to the nonpolar stationary phase of reversed-phase HPLC for separating the negatively charged DNA oligonucleotides. To address this problem, we attempted to utilize the Cy5-d15 and d19-FAM as standards based on their hydrophobic nature and polarity differences between Cy5 and FAM fluorophores. As shown in Figure 4a,b, the Cy5 and FAM fluorophores facilitated the separation of d15 and d19 in reversed-phase HPLC. The difference in the retention times of Cy5-d15 and d19-FAM was large enough to separate the two peaks for qualitative and quantitative analysis. Subsequently, Cy5-d15-BNSF-d19-FAM and Cy5-d15-BNSMB-d19-FAM (100 μM) were irradiated using a LED in 2× TAMg (pH 8.0) for 30 s. Afterward, the solvent was evaporated, and the residue was concentrated to 25 μL in volume for injecting into the HPLC system. Triplicate experiments were done on both samples, and the HPLC chromatograms are shown in Figures S71–S83. Calibration curves, as shown in Figures S84 and S85, were generated accordingly. By comparing the peak areas of uncaged products from Cy5-d15-BNSF-d19-FAM and Cy5-d15-BNSMB-d19-FAM, it was found that the one-photon uncaging efficiencies of BNSF- and BNSMB-conjugated DNA oligonucleotides were 97 ± 1 and 90 ± 3%, respectively. These were much higher as compared with those in the literature using a xenon lamp or mercury lamp.[44,45]

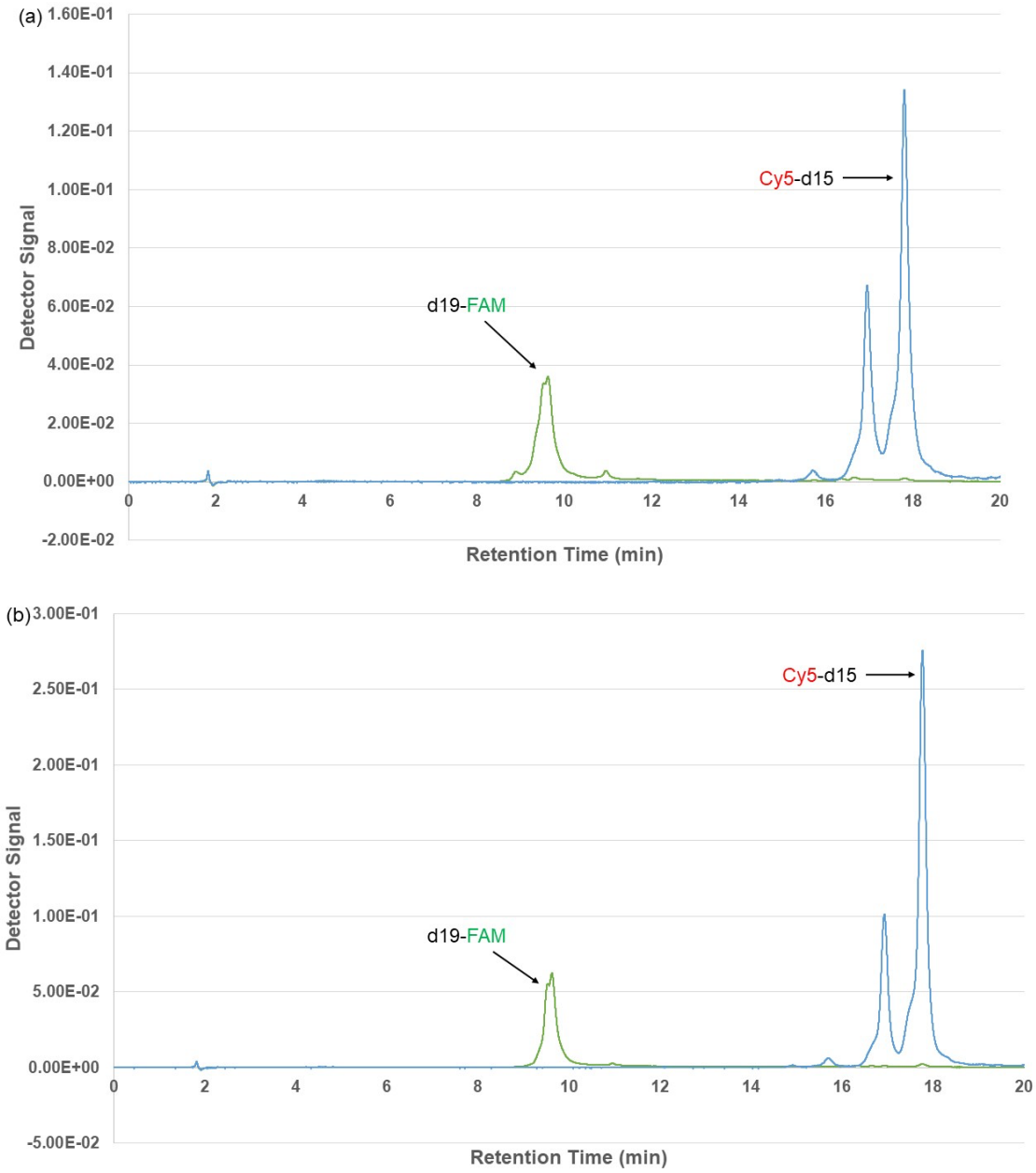

Figure 4. HPLC Chromatogram of (a) Cy5-d15-BNSF-d19-FAM (b) Cy5-d15-BNSMB-d19-FAM after irradiation by LED.

From the one-photon uncaging studies, both BNSF and BNSMB exhibited high-efficiency photolysis under visible light irradiation. The planarity of the chromophore, rigidity of the molecular structure, and steric hindrance raised by the BNSF motif might alter the hybridization of duplex DNAs. Therefore, the BNSMB motif was chosen for the construction of DNA-based logic gates.

3.5. Selective Photocleavage of PC spacer and BNSMB

To orthogonally activate the DNA logic devices, selective response of two photocleavable molecules to two particular wavelengths of light inputs is an important criterion. The PC spacer is an effective and commercially available photocleavage molecule activated by UV light at 365 nm, which is far away from the absorption region of BNSMB. Therefore, light inputs under the UV region and visible light region are used to activate our designed DNA devices with different logic operations. As shown in Figure 5a, the overall molecular structures of the PC spacer and BNSMB are not exactly the same; the PC spacer is a nitrobenzyl-based linker, whereas BNSMB is a nitrophenethyl linker.[56] Particularly, there is an additional methylene group on the benzylic carbon of the nitrobenzyl group in BNSMB, which makes the photolytic pathways of BNSMB significantly different from those of the PC spacer. Consequently, UV irradiation on the PC spacer converted the benzylic carbon of the nitrobenzyl group to *o*-nitrosoacetophenone, while the 2-(2-nitrophenyl)propyloxycarbonyl (NOPPC) motif in BNSMB was converted to *o*-nitrostyrene after photolysis.[57,58] To verify the selective cleavage of the PC spacer and BNSMB by light inputs of different wavelengths, a 24-base pair (bp) oligonucleotide inserted with these two molecules was synthesized and tested (5′-BHQ/GTTGTAAG/BNSMB/GTCAGCTA/PC/TGTACAAC-3′). Conjugation of the BHQ molecule at the 5′ end created a larger mass difference between photolyzed fragments (Figure 5b). Upon UV illumination, the PC spacer was cleaved to give a

DNA fragment with 8 bases and a DNA with 16 bases consisting of BHQ, BNSMB, and *o*-nitrosoacetophenone group. In denaturing PAGE analysis (lane 2 in Figure 5c), a DNA band was obtained with higher mobility than that of noncleaved DNA. However, the presence of the BNSMB molecule made the fragment migrate slower than that of a normal DNA strand with 16 bases. Irradiation of visible light resulted in two photolytic products including a DNA fragment with 8 bases and BHQ and another DNA fragment with 16 bases and a PC spacer. A DNA band was observed at a position near the DNA band of 16 bases in denaturing PAGE analysis (lane 3 in Figure 5c). Irradiations of both UV and visible lights completely cleaved the DNA into three 8-base fragments as expected. In general, the mobility of the DNA strand in PAGE analysis depends not only on its molecular weight and conformation but also on its polarity and hydrophilicity after molecular functionalization. The 8-base DNA fragments produced in lane 2 and lane 3 were too short and impossible to visualize after staining with Stains-All. Our observations are in agreement with previous studies.[37,39,59] Thus, the two 8-base DNA fragments are unobservable in Figure 5c. In contrast, the photolytic product of the 8-base DNA fragment consists of a nonpolar *o*-nitrosoacetophenone group in lane 4, which confers a mobility shift when compared to pure 8-base DNA strands or even DNA with longer lengths. Therefore, its mobility is a bit slower than that of the 16-base DNA fragment in lane 3. All these photolytic products were further characterized and confirmed by the MALDI-TOF mass analyses (Table S4 and Figures S86–S90). The results of mass characterization and denaturing PAGE analyses confirmed the selective and orthogonal photocleavage of PC-and BNSMB-functionalized DNA strands with two different wavelengths of lights.

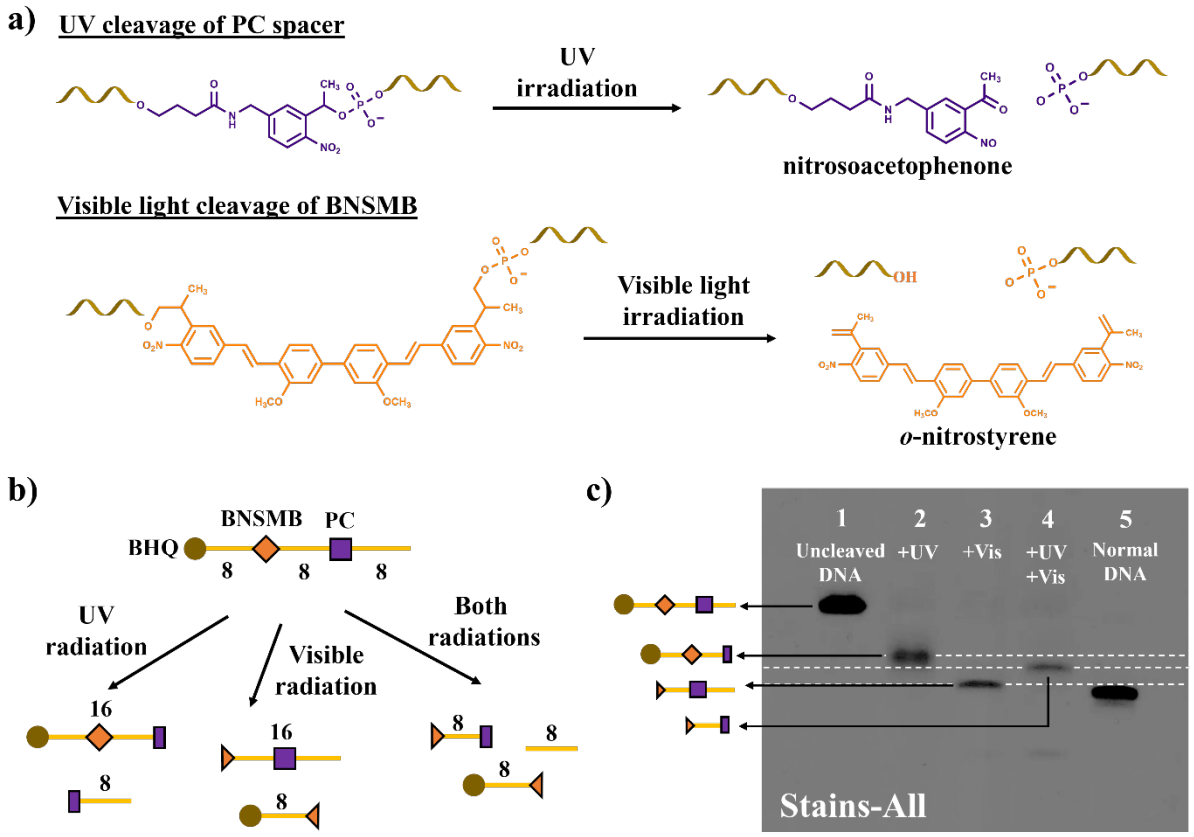

Figure 5. a) Schematic representation of photocleavage of PC spacer and BNSMB by UV and visible light respectively. b) Fragmentation of DNA containing PC spacer and BNSMB under different light irradiations. c) 20% denaturing gel electrophoresis analysis of b). Lane 1: non-cleaved DNA; lane 2: DNA cleaved by UV; lane 3: DNA cleaved by visible light; lane 4: DNA cleaved by UV and visible light; lane 5: normal DNA with 16 bases.

n our design, the logic devices are basically constructed by hybridizing two DNA oligonucleotides, namely **P-DNA** and **P-DNA′**, which are functionalized with the fluorophore Cy3, quencher, and two photocleavable molecules including PC and BNSMB at different positions. (0,0) represents the initial state without the input of radiations. (1,0) refers to the input of only UV radiation. Input of visible light only is indicated as (0,1), and (1,1) represents the input of both UV and visible lights. In response to the light irradiations, variation of Cy3 fluorescence creates an output signal

in the logic operations by changing the proximity between BHQ and Cy3 due to dehybridization of the duplex. In addition, the concept of molecular beacon (MB) formation is also introduced into the DNA logic gate systems. The self-hybridization of MB can hold Cy3 and BHQ in close proximity, which is an important conformational change in the operations of NOR and NAND gates to create a false output signal. The successful synthesis of all functionalized oligonucleotides was fully characterized by MALDI-TOF mass spectrometry (Figures S91–S102).

3.6.1 OR Gate

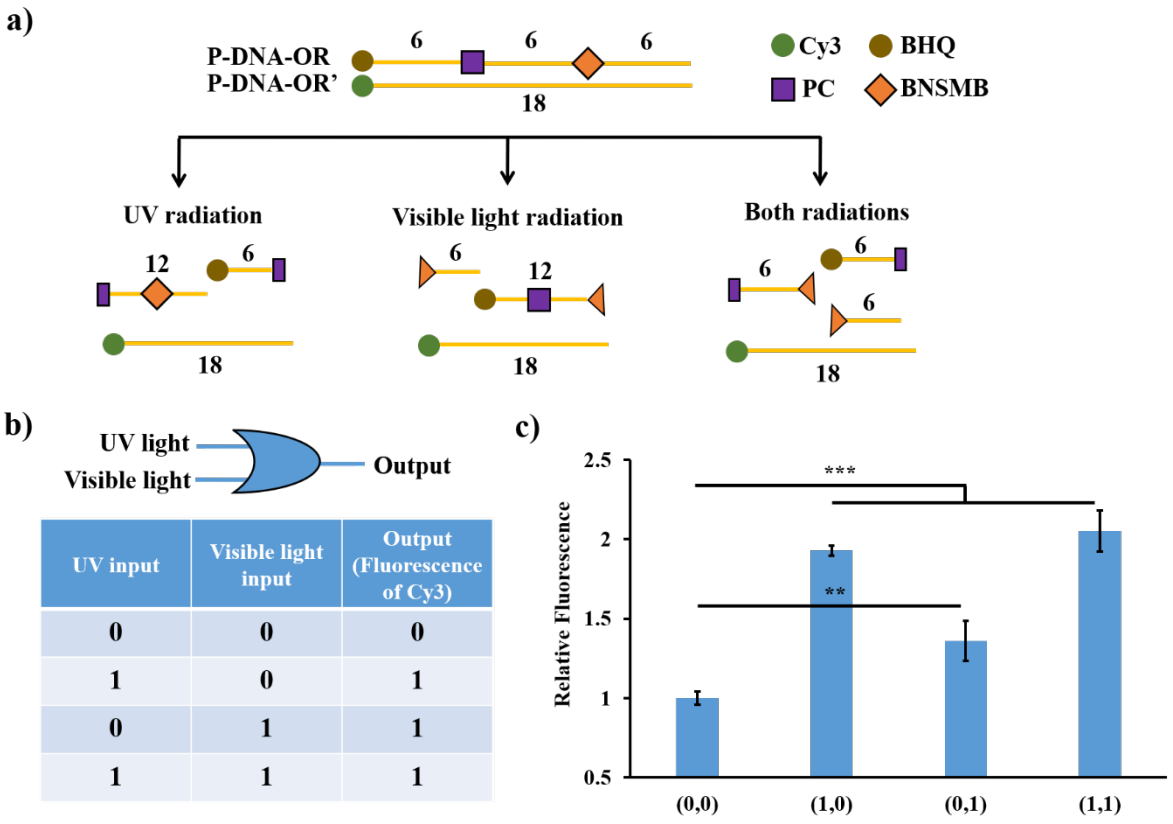

UV input	Visible light input	Output (Fluorescence of Cy3)
0	0	0
1	0	1
0	1	1
1	1	1

Figure 6. a) Schematic representation of OR gate under different light irradiations. b) The truth table of OR gate. c) The relative fluorescence of OR gate under different irradiations which the initial state was treated as 1. Data are presented in mean ± standard deviation (n = 3). **p < 0.01, ***p < 0.001, one-way ANOVA with the Tukey post hoc test.

The OR gate was designed as an 18-bp duplex by hybridizing BHQ-labeled **P-DNA-OR** and its Cy3-labeled complementary strands (**P-DNA-OR′**) (Figure 6a). The two photocleavable molecules including PC and BNSMB were inserted at every 6-base position on **P-DNA-OR**. Referring to the truth table of the OR gate, its output signal is true (1) when either one of the inputs is true (Figure 6b). At the initial state of the OR gate, the fluorescence emission of Cy3 on **P-DNA-OR′** was quenched due to the close proximity to BHQ as proved by fluorescence measurements and native PAGE analyses (lane 4 in Figure S103a,b). As a control, a C-OR duplex was also assembled without any photocleavable molecule (Figure S103a, lane 5). The initial quenched state of the OR gate was given as a false output signal (0), while the fluorescent state triggered by two light inputs was assigned as a true output signal (1). With UV irradiation applied, the DNA band of the designed OR gate disappeared and a new DNA band with higher mobility corresponding to the 18-mer **P-DNA-OR′** was observed (Figure S104, lane 3). It is noted that the PC spacer on **P-DNA-OR** underwent photolysis to generate a 6-base DNA fragment containing BHQ and a 12-base DNA fragment consisting of BNSMB. These two shorter DNA fragments were unstable and dissociated from the Cy3-labeled **P-DNA-OR′,** resulting in the restored fluorescence as an output signal (Figure 6c). In contrast, when visible light is applied, a new DNA band corresponding to **P-DNA-OR′** with higher mobility was observed and the fluorescence emission of Cy3 was restored (Figures 6c and S104, lane 4). These observations were attributed to the selective photocleavage of BNSMB to generate a 6-base DNA fragment and a 12-base DNA fragment consisting of PC and BHQ. Although a slight hybridization between a 12-bp PC-containing fragment and **P-DNA-OR′** was observed, the relative fluorescence intensity of Cy3 significantly increased ($p < 0.01$) by the input of (0,1). Subsequently, inputs of both light radiations led to a complete fragmentation of **P-DNA-OR** into three 6-base DNA fragments as both PC and PMSNB were cleaved. The Cy3-

labeled **P-DNA-OR′** was completely free from the BHQ molecules, resulting in the restored fluorescence emission of Cy3 (Figures 6c and S104, lane 5). No such DNA cleavage and no restoration of the fluorescence signal were observed in the C-OR duplex upon light irradiations (Figure S104). Importantly, the dependence of the readout signals of our DNA system based on the UV and visible light irradiations can imitate the function of signal communication in the OR logic gate.

3.6.2 NOR Gate

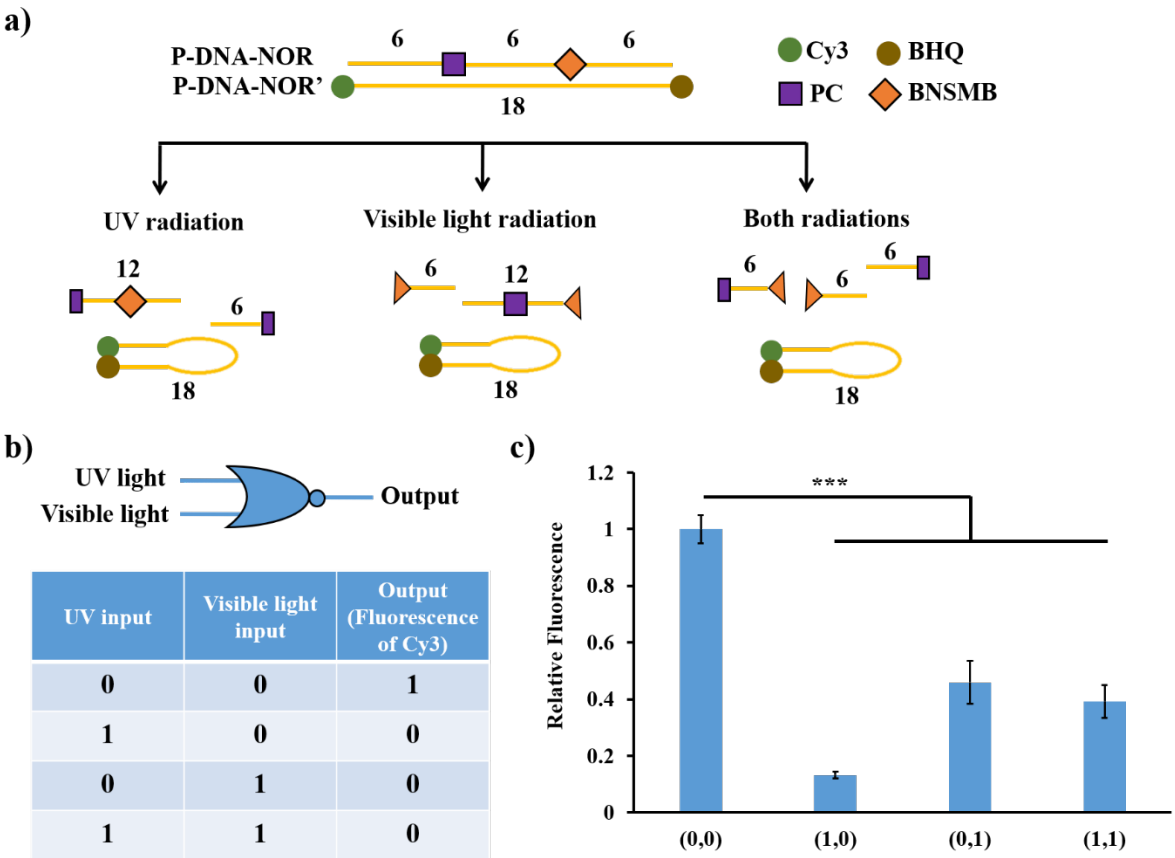

UV input	Visible light input	Output (Fluorescence of Cy3)
0	0	1
1	0	0
0	1	0
1	1	0

Figure 7. a) Schematic representation of NOR gate under different light irradiations. b) The truth table of NOR gate. c) The relative fluorescence of NOR gate under different irradiations which the

initial state was treated as 1. Data are presented in mean ± standard deviation (n = 3). ***$p < 0.001$, one-way ANOVA with the Tukey post hoc test.

The NOR gate was also designed as an 18-bp duplex by hybridizing the **P-DNA-NOR** strand and its complementary strand (**P-DNA-NOR′**), which was functionalized with Cy3 and BHQ at the 3′ and 5′ ends, respectively (Figures 7a and S105a, lane 4). Importantly, the sequence of **P-DNA-NOR′** was designed to self-assemble into the molecular beacon (MB) structure with low fluorescence when it was unhybridized (lane 3 in Figures S105a and S105b). As a control, a C-NOR duplex was also generated without any photocleavable molecule (Figure S105a, lane 5). Referring to the truth table of the NOR gate, the pattern of signal change in its operation is opposite to that of the OR gate. The output signal is only true (1) without any input. Otherwise, the output signal becomes false (0) when either single or both inputs are present (Figure 7b). At the initial state without any input (0,0), the fluorescence emission of Cy3 was at the highest level (Figures 7c and S106a, lane 2) as the distance between Cy3 and BHQ is far away by forming a duplex. When either UV or visible light was applied, a new DNA band with higher mobility corresponding to the MB formed and the emission of Cy3 was dramatically reduced. It is worth noting that 6-mer DNA fragments and 12-mer DNA fragments were generated by photocleavage of the PC spacer or BNSMB and then dissociated from **P-DNA-NOR′**. This selective photolysis would promote the self-hybridization of **P-DNA-NOR′** into a MB structure with the close proximity of Cy3 and BHQ. Similar results were obtained when the reaction system was irradiated with both light inputs. This is because the PC spacer and BNSMB were simultaneously cleaved, and then, three 6-mer DNA fragments were unhybridized from **P-DNA-NOR′**, giving rise to a diminished fluorescence by forming the MB structure (Figures 7c and S106a, lane 5). In contrast, there is no significant decrease of the fluorescence emission signal of Cy3, and no MB structure was formed in the C-

NOR duplex (Figures S106 and S107). Overall, the result of native PAGE analysis was consistent with that of the fluorescence studies. Through normalizing the intensity detected in the NOR gate with that of the control C-NOR duplex, the relative fluorescence in the outputs of (0,1) and (1,1) was suppressed. The output signals of (0,1) and (1,1) were both considered false.

3.6.3. AND Gate

Using a similar strategy, 24-mer **P-DNA-AND** was designed and functionalized with PC and BMSMB at every 8-base position and with two BHQ molecules at both ends. Its complementary strand **P-DNA-AND′** was modified with two fluorophores at both terminals and further hybridized with **P-DNA-AND** to form an AND gate as a 24-mer duplex (Figures 8a and S108a, lane 4). Referring to the truth table of the AND gate, a true output signal is produced only when both inputs are true. Input of either one false signal would result in a false output signal (Figure 8b). At the initial state without any light input, the fluorescence signal of the two fluorophores was completely quenched by the two BHQ molecules (Figure S108b). When either UV or visible light input is applied to the reaction systems, the PC spacer or BNSMB was photocleaved, respectively, to generate an 8-mer BHQ-labeled DNA fragment dissociated from the **P-DNA-AND′** strand. The resulting partially hybridized DNA complex was still stable enough to maintain the quenching effects, leading to low fluorescence intensity of the fluorophores. In contrast, upon irradiation of two light inputs, both the PC spacer and BNSMB were completely cleaved to release three 8-mer DNA fragments, while the two fluorophores on **P-DNA-AND′** were free from BHQ molecules. This photolysis by two light inputs would result in at least twofold enhancement of the fluorescence intensity of fluorophores (Figure 8c), and a clear fluorescence signal in the native PAGE analysis is shown in Figure S109, lane 5. No such fluorescence enhancement is observed in a control C-AND duplex (without functionalization of photocleavable

molecules) in response to the two light inputs as shown in Figure S109. Importantly, an immense increase of fluorescence signals was observed by both light irradiations with the output of (1,1), which became differentiable to those of states at (1,0) and (0,1). The output of (1,1) was considered a true signal, while the others were false. In our design, the dependence of the readout signals based on both UV and visible light irradiations can mimic the function of signal communication in AND logic gates.

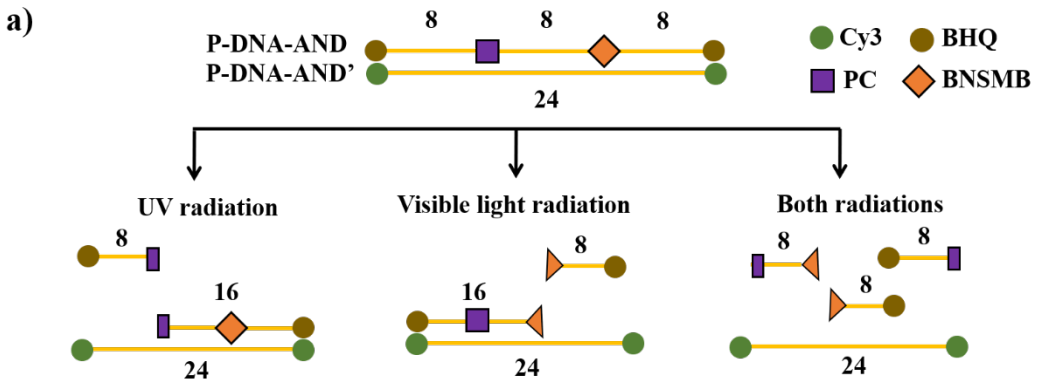

b)

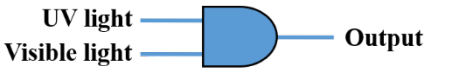

UV Input	Visible light Input	Output (Fluorescence of Cy3)
0	0	0
1	0	0
0	1	0
1	1	1

c)

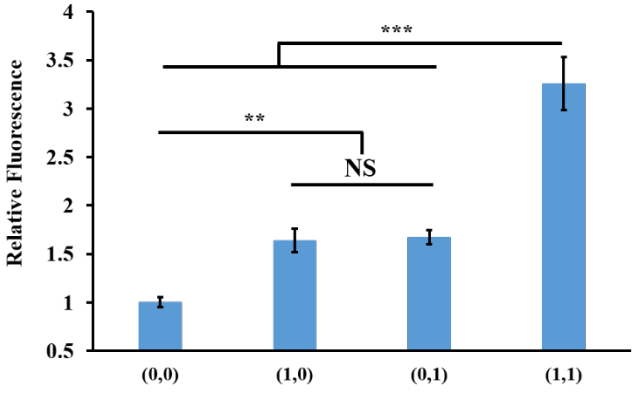

Figure 8. a) Schematic representation of AND gate under different light irradiations. b) The truth table of AND gate. c) The relative fluorescence of AND gate under different irradiations which the initial state was treated as 1. Data are presented in mean ± standard deviation (n = 3). **p < 0.01, ***p < 0.001, one-way ANOVA with the Tukey post hoc test.

3.6.4 NAND Gate

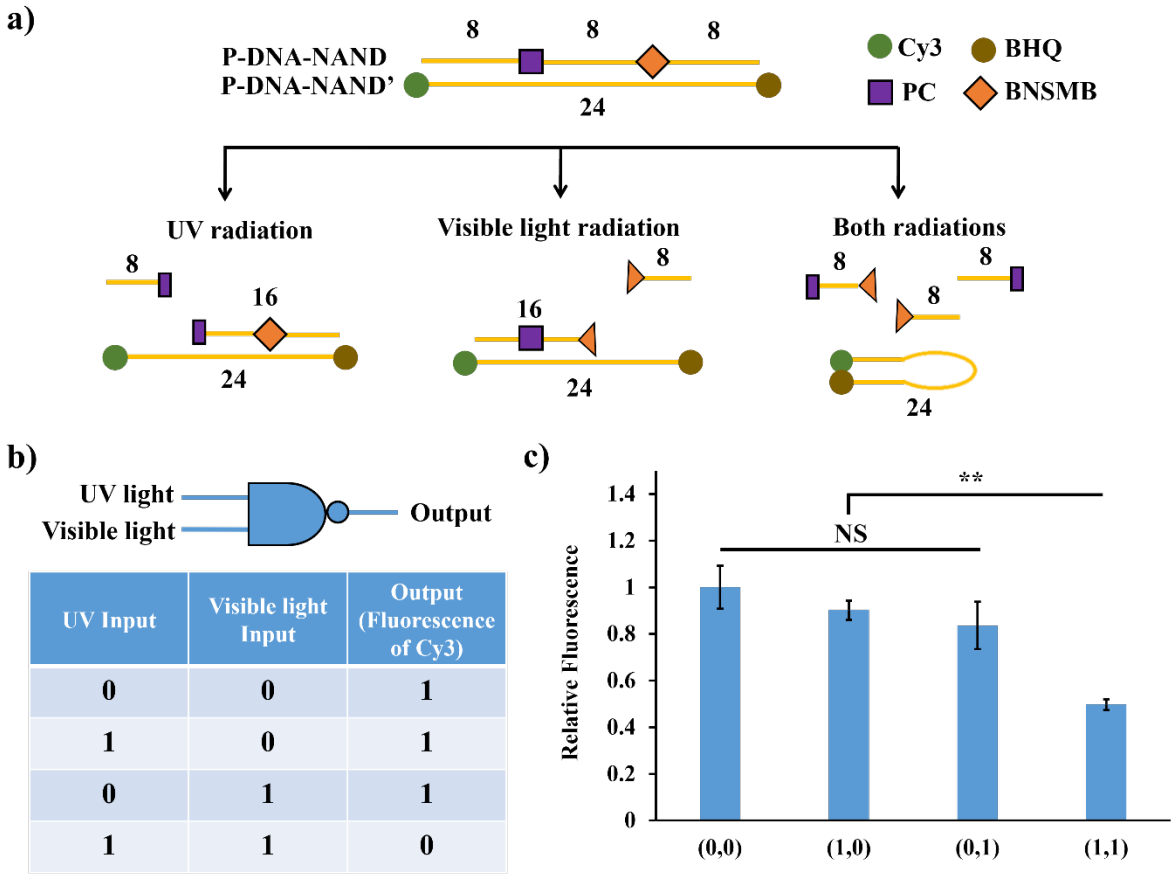

UV Input	Visible light Input	Output (Fluorescence of Cy3)
0	0	1
1	0	1
0	1	1
1	1	0

Figure 9. a) Schematic representation of NAND gate under different light irradiations. b) Truth table of NAND gate. c) The relative fluorescence of NAND gate under different irradiations which the initial state was treated as 1. Data are presented in mean ± standard deviation (n = 3). **p < 0.01, one-way ANOVA with the Tukey post hoc test.

The pattern of output signals in the operation of the NAND gate is just the reverse of that of the AND gate. In our design, the construction of the NAND gate comprised the components in the AND gate and NOR gate. The length of the duplex was kept as 24 bp, and the DNA sequences were the same as those of the AND gate to ensure the hybridization between the fragments, while

the complementary strand can be maintained when a single input is present. The PC spacer and BNSMB molecules were functionalized at every 8-base position on the **P-DNA-NAND** strand, while Cy3 and BHQ were conjugated to the 3′ and 5′ ends of its complementary strand **P-DNA-NAND′**, respectively (Figures 9a and S110a, lane 4). Referring to the truth table of the NAND gate, the output signal is only false when both of the input signals are true (Figure 9b). A strong fluorescence was detected at the initial state of the NAND gate without inputs, which was treated as a true output signal (Figures 9c and S110b). By irradiating with either UV or visible light, the PC spacer or BNSMB was photocleaved, respectively, to generate a short 8-mer DNA fragment, which is not stable enough to hybridize with **P-DNA-NAND′**. Meanwhile, the resulting 16-mer DNA fragment is still able to hybridize with 24-mer **P-DNA-NAND′** to prevent the formation of the MB structure of **P-DNA-NAND′**. Consequently, the fluorescence intensities of Cy3 detected as the output of the NAND gate at inputs of (1,0) and (0,1) are observed at a high level, which showed no significant difference to the NAND gate at the initial state ($p > 0.5$) (Figures 9c and S111). The output signals of (1,0) and (0,1) were both considered true. In contrast, a new DNA band with higher mobility was formed and the fluorescence emission of Cy3 was dramatically reduced upon both UV and visible light irradiations. These results are attributed to the simultaneous photocleavage of the PC spacer and BMSNB molecules and generation of three 8-mer DNA fragments dissociated from **P-DNA-NAND′**. This would promote the self-hybridization of **P-DNA-NAND′** into a MB structure with the close proximity of Cy3 and BHQ. The output signal of (1,1) became false. The fluorescence variation of the DNA system response to the UV and visible lights matched the logic operation pattern of the NAND gate. Consequently, the dependence of the readout signals based on the two light inputs can mimic the function of signal communication in NAND logic gates.

Conclusions

In summary, we successfully synthesized two 400 nm light-activated phosphoramidites based on the BNSF and BNSMB structures as photocleavable linkers for oligonucleotide conjugation. The BNSF- and BNSMB-functionalized DNA oligonucleotides showed fast and efficient one-photon uncaging properties by cleavage of photolabile bonds of NPPOC PPGs, resulting in short pieces of DNA fragments. BNSF-functionalized DNAs have also shown two-photon sensibility at 800 nm. Together with UV-cleavable molecules, photoregulated DNA devices were further designed and constructed as duplex structures, which are functionalized with fluorophores, a quencher, and two photocleavable molecules including PC and BNSMB molecules. Selective cleavage of PC and BNSMB is achieved in response to UV and visible light irradiations, respectively, as two inputs. This results in the controllable dissociation of pieces of DNA fragments, then followed by changes of fluorescence emission as signal outputs in the reaction systems. By tuning the number and position of the photocleavable molecules, fluorophores, and quenchers, various DNA devices were developed, in which they mimic the functions of Boolean logic gates and achieve logic operations in AND, OR, NOR, and NAND gates in response to light inputs of two different wavelengths. By sequence design, oligonucleotides with antisense or aptamer sequences can be precisely programmed in DNA devices and triggered to release in a selective or sequential manner by irradiation of certain wavelengths of lights. Therefore, this DNA device shows potential as a wavelength-dependent drug delivery system for selective control over the release of multiple individual therapeutic oligonucleotide-based drugs such as aptamers, microRNA mimics, antagomirs, DNAzymes, DNA decoys, and synthetic guide strands for CRISPR/Cas. We strongly believe that our work enriches the library of photocleavable phosphoramidites available for

bioconjugation and paves the way for constructing wavelength-selective, orthogonal-regulated DNA-based logic devices for applications in materials science, polymers, chemistry, and biology.

ASSOCIATED CONTENT

Supporting Information

The supporting information is available free of charge at ACS publication website with DOI of . Synthetic schemes and NMR spectra of photocleavable molecules, MALDI-TOF spectra of all functionalized oligonucleotides, HPLC chromatograms of photolytic products, two-photon uncaging results, fluorescence spectra and gel electrophoresis are included in the supporting information.

AUTHOR INFORMATION

Corresponding Author

Pik Kwan Lo peggylo@cityu.edu.hk*

Frédéric Bolze frederic.bolze@unistra.fr*

Alexandre Specht alexandre.specht@unistra.fr*

Author Contributions

L. S. Liu, H. M. Leung, F. Bolze, A. Specht and P. K. Lo designed the project; L. S. Liu synthesized the photocleavable molecules and functionalized oligonucleotides; UV-Vis absorption in qualitative analysis and two-photon uncaging study were performed by C. Morville, F. Bolze and

A. Specht. Gel electrophoretic analysis was done by H. M. Leung and H. C. Chu; Quantification of photolytic products was done by L. S. Liu, H. M. Leung and J. Y. Tee; Formation and operation of DNA logic gates were performed by H. M. Leung and H. C. Chu; L. S. Liu, H. M. Leung, F. Bolze, A. Specht and P. K. Lo analyzed the data; F. Bolze, A. Specht and P. K. Lo supervised the project. L. S. Liu, H. M. Leung, F. Bolze, A. Specht and P. K. Lo wrote the manuscript with contributions of all authors. All authors have given approval to the final version of the manuscript. ‡ L. S. Liu and H. M. Leung contributed equally.

Notes

The authors declare no competing financial interest.

ACKNOWLEDGMENT

This work was supported by Health and Medical Research Fund (07181396 and 05160336), by National Science Foundation of China (21574109 and 217780430), by Hong Kong Research Grants Council 11301220, 11304719, by City University of Hong Kong 9680104 and 7004911, by the Université de Strasbourg, by the CNRS, and by a Grant from the Agence Nationale de la Recherche (Contract No. ANR-18-CE09-0016-01).

REFERENCE

(1) Wolffenbuttel, R. F. On-Chip Functional Integration. In Silicon Sensors and Circuits: On-chip Compatibility, 1st ed.; Chapman & Hall, 1996; pp 1–54.

(2) Meijer, G. Silicon Sensors: An Introduction. In Smart Sensor Systems, 1st ed.; John Wiley & Sons,, 2008; pp; pp 55–78.

(3) Ball, P. Chemistry Meets Computing. Nature 2000, 406, 118–120.

(4) Lloyd, S. Ultimate Physical Limits to Computation. Nature 2000, 406, 1047–1054.

(5) Liu, L.; Liu, P.; Ga, L.; Ai, J. Advances in Applications of Molecular Logic Gates. ACS Omega 2021, 6, 30189–30204.

(6) Xu, X.; Shang, Y.; Liu, F.; Jiang, Q.; Ding, B. Logic Devices Based on Nucleic Acid Self-Assembly. InfoMat 2021, 3, 1070–1082.

(7) Fan, D.; Wang, J.; Wang, E.; Dong, S. Propelling DNA Computing with Materials' Power: Recent Advancements in Innovative DNA Logic Computing Systems and Smart Bio-Applications. Adv. Sci. 2020, 7, No. 2001766.

(8) Ma, Q.; Zhang, C.; Zhang, M.; Han, D.; Tan, W. DNA Computing: Principle, Construction, and Applications in Intelligent Diagnostics. Small Structures 2021, 2, No. 2100051.

(9) Liu, X.; Aizen, R.; Freeman, R.; Yehezkeli, O.; Willner, I. Multiplexed Aptasensors and Amplified DNA Sensors Using Functionalized Graphene Oxide: Application for Logic Gate Operations. ACS Nano 2012, 6, 3553–3563.

(10) Zhu, Q. Y.; Zhang, F. R.; Du, Y.; Zhang, X. X.; Lu, J. Y.; Yao, Q. F.; Huang, W. T.; Ding, X. Z.; Xia, L. Q. Graphene-Based Steganographically Aptasensing System for Information Computing, Encryption and Hiding, Fluorescence Sensing and in Vivo Imaging of Fish Pathogens. ACS Appl. Mater. Interfaces 2019, 11, 8904–8914.

(11) Wang, Q.; Yang, Q.; Wu, W. Graphene-Based Steganographic Aptasensor for Information Computing and Monitoring Toxins of Biofilm in Food. Front. Microbiol. 2020, 10, 3139.

(12) Adleman, L. M. Molecular Computation of Solutions to Combinatorial Problems. Science 1994, 266, 1021–1024.

(13) Shi, Y.; Sun, H.; Xiang, J.; Chen, H.; Yang, Q.; Guan, A.; Li, Q.; Yu, L.; Tang, Y. Construction of DNA Logic Gates Utilizing a H+/Ag + Induced i-motif Structure. Chem. Commun. 2014, 50, 15385–15388.

(14) Guo, Y.; Zhou, L.; Xu, L.; Zhou, X.; Hu, J.; Pei, R. Multiple Types of Logic Gates Based on a Single G-Quadruplex DNA Strand. Sci. Rep. 2014, 4, No. 7315.

(15) Zhu, J.; Zhang, L.; Zhou, Z.; Dong, S.; Wang, E. Molecular Aptamer Beacon Tuned DNA Strand Displacement to Transform Small Molecules into DNA Logic Outputs. Chem. Commun. 2014, 50, 3321–3323.

(16) Elbaz, J.; Wang, F.; Remacle, F.; Willner, I. pH-Programmable DNA Logic Arrays Powered by Modular DNAzyme Libraries. Nano Lett. 2012, 12, 6049–6054.

(17) Pei, H.; Liang, L.; Yao, G.; Li, J.; Huang, Q.; Fan, C. Reconfigurable Three-Dimensional DNA Nanostructures for the Construction of Intracellular Logic Sensors. Angew. Chem., Int. Ed. 2012, 51, 9020–9024.

(18) Yoshida, W.; Yokobayashi, Y. Photonic Boolean Logic Gates Based on DNA Aptamers. Chem. Commun. 2007, 2, 195–197.

(19) Zhu, J.; Zhang, L.; Zhou, Z.; Dong, S.; Wang, E. Aptamer-Based Sensing Platform Using Three-Way DNA Junction-Driven Strand Displacement and Its Application in DNA Logic Circuit. Anal. Chem. 2014, 86, 312–316.

(20) Zhu, J.; Zhang, L.; Li, T.; Dong, S.; Wang, E. Enzyme-Free Unlabeled DNA Logic Circuits Based on Toehold-Mediated Strand Displacement and Split G-Quadruplex Enhanced Fluorescence. Adv. Mater. 2013, 25, 2440–2444.

(21) Li, W.; Yang, Y.; Yan, H.; Liu, Y. Three-Input Majority Logic Gate and Multiple Input Logic Circuit Based on DNA Strand Displacement. Nano Lett. 2013, 13, 2980–2988.

(22) Chen, Y.; Song, Y.; Wu, F.; Liu, W.; Fu, B.; Feng, B.; Zhou, X. A DNA Logic Gate Based on Strand Displacement Reaction and Rolling Circle Amplification, Responding to Multiple Low-Abundance DNA Fragment Input Signals, and Its Application in Detecting miRNAs. Chem. Commun. 2015, 51, 6980–6983.

(23) Li, L.; Zhang, W.; Tang, X.; Li, Z.; Wu, Y.; Xiao, X. Fine and Bidirectional Regulation of Toehold-Mediated DNA Strand Displacement by a Wedge-Like DNA Tool. Chem. Commun. 2020, 56, 8794–8797.

(24) Chen, J.; Pan, J.; Chen, S. A Label-Free and Enzyme-Free Platform with a Visible Output for Constructing Versatile Logic Gates Using Caged G-Quadruplex as the Signal Transducer. Chem. Sci. 2018, 9, 300–306.

(25) Park, K. S.; Seo, M. W.; Jung, C.; Lee, J. Y.; Park, H. G. Simple and Universal Platform for Logic Gate Operations Based on Molecular Beacon Probes. Small 2012, 8, 2203–2212.

(26) Liu, Q.; Deiters, A. Optochemical Control of Deoxyoligonucleotide Function via a Nucleobase-Caging Approach. Acc. Chem. Res. 2014, 47, 45–55.

(27) Xing, C.; Chen, Z.; Dai, J.; Zhou, J.; Wang, L.; Zhang, K.-L.; Yin, X.; Lu, C.; Yang, H. Light-Controlled, Toehold-Mediated Logic Circuit for Assembly of DNA Tiles. ACS Appl. Mater. Interfaces 2020, 12, 6336–6342.

(28) Prokup, A.; Hemphill, J.; Deiters, A. DNA Computation: A Photochemically Controlled AND Gate. J. Am. Chem. Soc. 2012, 134, 3810–3815.

(29) Song, X.; Eshra, A.; Dwyer, C.; Reif, J. Renewable DNA Seesaw
Logic Circuits Enabled by Photoregulation of Toehold-Mediated Strand Displacement. RSC Adv. 2017, 7, 28130–28144.

(30) Chen, S.; Xu, Z.; Yang, W.; Lin, X.; Li, J.; Li, J.; Yang, H. Logic- Gate-Actuated DNA-Controlled Receptor Assembly for the Programmable Modulation of Cellular Signal Transduction. Angew. Chem., Int. Ed. 2019, 58, 18186–18190.

(31) Li, F.; Chen, H.; Pan, J.; Cha, T.-G.; Medintz, I. L.; Choi, J. H. A DNAzyme-Mediated Logic Gate for Programming Molecular Capture and Release on DNA Origami. Chem. Commun. 2016, 52, 8369–8372.

(32) Hemphill, J.; Deiters, A. DNA Computation in Mammalian Cells: MicroRNA Logic Operations. J. Am. Chem. Soc. 2013, 135, 10512–10518.

(33) Emanuelson, C.; Bardhan, A.; Deiters, A. DNA Computing: NOT Logic Gates See the Light. ACS Synth. Biol. 2021, 10, 1682– 1689.

(34) Xiong, X.; Xiao, M.; Lai, W.; Li, L.; Fan, C.; Pei, H. Optochemical Control of DNA-Switching Circuits for Logic and Probabilistic Computation. Angew. Chem., Int. Ed. 2021, 60, 3397–3401.

(35) Wang, S.; He, B.; Ren, W.; Suo, Z.; Xu, Y.; Wei, M.; Jin, H. Triple-Helix Molecular Switch Triggered Cleavage Effect of DNAzyme for Ultrasensitive Electrochemical Detection of Chloramphenicol. ACS Appl. Mater. Interfaces 2022, 14, 24681–24689.

(36) Zhou, X.; Lin, S.; Yan, H. Interfacing DNA Nanotechnology and Biomimetic Photonic Complexes: Advances and Prospects in Energy and Biomedicine. J. Nanobiotechnol. 2022, 20, 257.

(37) Tam, D. Y.; Dai, Z.; Chan, M. S.; Liu, L. S.; Cheung, M. C.; Bolze, F.; Tin, C.; Lo, P. K. A Reversible DNA Logic Gate Platform Operated by One- and Two-Photon Excitations. Angew. Chem., Int. Ed. 2016, 55, 164–168.

(38) Chaud, J.; Morville, C.; Bolze, F.; Garnier, D.; Chassaing, S.; Blond, G.; Specht, A. Two-Photon Sensitive Coumarinyl Photoremovable Protecting Groups with Rigid Electron-Rich Cycles Obtained by Domino Reactions Initiated by a 5-exo-Dig Cyclocarbopalladation. Org. Lett. 2021, 23, 7580–7585.

(39) Li, L.; Tong, R.; Chu, H.; Wang, W.; Langer, R.; Kohane, D. S. Aptamer Photoregulation In Vivo. Proc. Natl. Acad. Sci. U.S.A. 2014, 111, 17099–17103.

(40) Xu, C.; Li, H.; Zhang, K.; Binzel, D. W.; Yin, H.; Chiu, W.; Guo, P. Photo-Controlled Release of Paclitaxel and Model Drugs from RNA Pyramids. Nano Res. 2019, 12, 41–48.

(41) Chen, X.; Qiu, L.; Cai, R.; Cui, C.; Li, L.; Jiang, J.-h.; Tan, W. Aptamer-Directed Protein-Specific Multiple Modifications of Membrane Glycoproteins on Living Cells. ACS Appl. Mater. Interfaces 2020, 12, 37845–37850.

(42) Olson, J. P.; Banghart, M. R.; Sabatini, B. L.; Ellis-Davies, G. C. R. Spectral Evolution of a Photochemical Protecting Group for Orthogonal Two-Color Uncaging with Visible Light. J. Am. Chem. Soc. 2013, 135, 15948–15954.

(43) Zhang, D.; Zhou, C. Y.; Busby, K. N.; Alexander, S. C.; Devaraj, N. K. Light-Activated Control of Translation by Enzymatic Covalent mRNA Labeling. Angew. Chem., Int. Ed. 2018, 57, 2822–2826.

(44) Bojtár, M.; Németh, K.; Domahidy, F.; Knorr, G.; Verkman, A.; Kállay, M.; Kele, P. Conditionally Activatable Visible-Light Photocages. J. Am. Chem. Soc. 2020, 142, 15164–15171.

(45) Chitose, Y.; Abe, M.; Furukawa, K.; Lin, J.-Y.; Lin, T.-C.; Katan, C. Design and Synthesis of a Caged Carboxylic Acid with a Donor–π–Donor Coumarin Structure: One-Photon and Two-Photon Uncaging Reactions Using Visible and Near-Infrared Lights. Org. Lett. 2017, 19, 2622–2625.

(46) Bojtár, M.; Kormos, A.; Kis-Petik, K.; Kellermayer, M.; Kele, P. Green-Light Activatable, Water-Soluble Red-Shifted Coumarin

Photocages. Org. Lett. 2019, 21, 9410–9414.

(47) Gandioso, A.; Contreras, S.; Melnyk, I.; Oliva, J.; Nonell, S.; Velasco, D.; García-Amorós, J.; Marchán, V. Development of Green/ Red-Absorbing Chromophores Based on a Coumarin Scaffold That Are Useful as Caging Groups. J. Org. Chem. 2017, 82, 5398–5408.

(48) Gug, S.; Bolze, F.; Specht, A.; Bourgogne, C.; Goeldner, M.; Nicoud, J.-F. Molecular Engineering of Photoremovable Protecting Groups for Two-Photon Uncaging. Angew. Chem., Int. Ed. 2008, 47, 9525–9529.

(49) Olejniczak, J.; Sankaranarayanan, J.; Viger, M. L.; Almutairi, A. Highest Efficiency Two-Photon Degradable Copolymer for Remote Controlled Release. ACS Macro Lett. 2013, 2, 683–687.

(50) Dai, Z.; Tam, D. Y.; Xu, H.; Chan, M. S.; Liu, L. S.; Bolze, F.; Sun, X. H.; Lo, P. K. Conformational Change of Self-Assembled DNA Nanotubes Induced by Two-Photon Excitation. Small 2015, 11, 4090–4096.

(51) Chan, M. S.; Tam, D. Y.; Dai, Z.; Liu, L. S.; Ho, J. W.-T.; Chan, M. L.; Xu, D.; Wong, M. S.; Tin, C.; Lo, P. K. Mitochondrial Delivery of Therapeutic Agents by Amphiphilic DNA Nanocarriers. Small 2016, 12, 770–781.

(52) Dai, Z.; Lo, P. K. Photo-Switchable Patterning of Gold

Nanoparticles Along 3D DNA Nanotubes. Nanoscale 2018, 10, 5431–5435.
(53) Roy, B.; Roy, S.; Kundu, M.; Maji, S.; Pal, B.; Mandal, M.;
Singh, N. D. P. Ground-State Proton-Transfer (GSPT)-Assisted Enhanced Two-Photon Uncaging from a Binol-Based AIE-Fluoro- genic Phototrigger. Org. Lett. 2021, 23, 2308–2313.
(54) Gug, S.; Charon, S.; Specht, A.; Alarcon, K.; Ogden, D.; Zietz, B.; Léonard, J.; Haacke, S.; Bolze, F.; Nicoud, J.-F.; Goeldner, M. Photolabile Glutamate Protecting Group with High One- and Two-Photon Uncaging Efficiencies. ChemBioChem 2008, 9, 1303–1307.
(55) Weyel, X. M. M.; Fichte, M. A. H.; Heckel, A. A Two-Photon- Photocleavable Linker for Triggering Light-Induced Strand Breaks in Oligonucleotides. ACS Chem. Biol. 2017, 12, 2183–2190.
(56) Goeldner, M.; Givens, R. Photoremovable Protecting Groups Used for the Caging of Biomolecule. In Dynamic Studies in Biology: Phototriggers, Photoswitches and Caged Biomolecules, Vol. 1; Wiley-VCH, 2005; pp 1–94.
(57) Klán, P.; Šolomek, T.; Bochet, C. G.; Blanc, A.; Givens, R.; Rubina, M.; Popik, V.; Kostikov, A.; Wirz, J. Photoremovable Protecting Groups in Chemistry and Biology: Reaction Mechanisms and Efficacy. Chem. Rev. 2013, 113, 119–191.
(58) Mikkelsen, R. J. T.; Grier, K. E.; Mortensen, K. T.; Nielsen, T. E.; Qvortrup, K. Photolabile Linkers for Solid-Phase Synthesis. ACS Comb. Sci. 2018, 20, 377–399.
(59) Zhao, D.; Yang, G.; Liu, Q.; Liu, W.; Weng, Y.; Zhao, Y.; Qu, F.; Li, L.; Huang, Y. A Photo-Triggerable Aptamer Nanoswitch for Spatiotemporal Controllable siRNA Delivery. Nanoscale 2020, 12, 10939–10943.